Low-temperature far-infrared study of localized states in In-doped $Pb_{0.75}Sn_{0.25}Te$ single crystals



1992 J. Phys.: Condens. Matter 4 4323

(http://iopscience.iop.org/0953-8984/4/17/012)

J. Phys.: Condens. Matter 4 (1992) 4323–4330. Printed in the UK

# Low-temperature far-infrared study of localized states in In-doped $Pb_{0.75}Sn_{0.25}Te$ single crystals

N Romčević†, Z V Popović† and D R Khokhlov‡

† Institute of Physics, PO Box 57, 11001 Belgrade, Yugoslavia

‡ Low-Temperature Physics Department, Moscow State University, 117234 Moscow, Russia

Received 5 December 1991

**Abstract.** We present low-temperature far-infrared reflection spectra of In-doped $Pb_{0.75}Sn_{0.25}Te$ single crystals at various doping concentrations. These spectra at temperatures below 20 K are fitted using a modified plasmon–phonon interaction model with an additional oscillator, which describes the electron transition from two- to one-electron states at the In impurity level. The In-doped $Pb_{0.75}Sn_{0.25}Te$ impurity-state energy structure is explained.

## 1. Introduction

$Pb_{1-x}Sn_xTe$ is a well known narrow-band-gap semiconductor [1] with a usually very high ($n, p > 10^{17}$ cm$^{-3}$) intrinsic free-carrier concentration. In $A^{IV}B^{VI}$ alloys, indium concentrations higher than those of other donors and acceptors result in an impurity level the location of which is determined by alloy composition and temperature [2, 3]. The Fermi level of $A^{IV}B^{VI}$ alloys is pinned to the In impurity level and shifts with it on temperature and pressure changes [2]. Even though the pinning of the Fermi level to the In impurity level has been studied extensively [4, 5], no satisfactory explanation of this effect exists as yet. For $0.28 > x > 0.22$ the In impurity level lies within the forbidden band (dielectric states [2]), resulting in a sharp drop in the free-carrier concentration. These In-doped alloys are unique in that (at temperatures below about 20 K in the dielectric state) they are photosensitive and exhibit a decrease in electrical resistivity of several orders of magnitude when illuminated by low-intensity infrared radiation [6].

Because of their high free-carrier concentration, the optical properties of In-doped $Pb_{1-x}Sn_xTe$ in the far-infrared (FIR) spectral region have usually been investigated on thin-film samples [7] where a temperature-induced plasma frequency shift has been observed.

In our earlier paper [8] we analysed the FIR reflection spectra of a 0.5 at.% In-doped $Pb_{0.75}Sn_{0.25}Te$ single crystal and showed that, if a photo-excited free-carrier concentration spatial distribution is introduced into the plasmon–phonon interaction model, good agreement is obtained between the experimental and theoretical spectra. FIR spectra of the 1.2 at.% In-doped $Pb_{0.75}Sn_{0.25}Te$ single crystal are given in [9]. These spectra were analysed using a fitting procedure based on the plasmon–phonon interaction model. Below 20 K, a new structure is in evidence that has to be fitted

0953-8984/92/174323+08$04.50  

by an additional oscillator in the plasmon–phonon interaction model. It may be explained in terms of $Pb_{0.75}Sn_{0.25}Te$ (In) localized impurity states.

In this paper, we present FIR reflection spectra of both 0.5 at.% and 1.2 at.% In-doped $Pb_{0.75}Sn_{0.25}Te$ single crystals from 50 to 250 $cm^{-1}$ at temperatures of 5–20 K. The FIR spectra change with the In content and the infrared irradiating flux. These spectra are also analysed using a fitting procedure based on the modified plasmon–phonon interaction model (but incorporating an additional oscillator characterizing localized impurity states). Thus, the location of the impurity level at $T = 0$ K, the temperature $T_k$ at which this level appears and its temperature dependence are obtained. The potential barrier width between localized states at $T = 0$ K and its value versus temperature as well as impurity-state-filling mechanisms are determined.

## 2. Experimental details

Indium-doped $Pb_{0.75}Sn_{0.25}Te$ single crystals grown by the modified Bridgman method were studied. Details of both the growth procedure and the measurement may be found in [8, 9]. A Bruker IFS 113v spectrometer with Oxford model CF 100 cryostat was used for the low-temperature FIR reflectivity measurements.

## 3. Results and discussion

Work to date on the persistent photoconductivity effect in In-doped $Pb_{0.75}Sn_{0.25}Te$ indicates that the effect occurs at temperatures below about 20 K, that it is most pronounced at indium concentrations of about 0.5 at.% and that the effect weakens with further increase in indium concentration [10]. Moreover, the quasi-stationary photo-excited carrier concentration is proportional to the incident irradiating flux $\Phi$, if other parameters are constant. In an attempt to gain insight into how all the above are demonstrated in In-doped $Pb_{0.75}Sn_{0.25}Te$ reflection spectra, we present FIR reflectivity spectra at $T = 10$ K: figure 1(*a*) for 1.2 at.% In, figure 1(*b*) the same as for figure 1(*a*) but at $\Phi_2 = 0.75\Phi_1$ (a decrease in irradiation flux effected by a sample holder with a 25% smaller diaphragm surface) and figure 1(*c*) for 0.5 at.% In and $\Phi_3 = \Phi_1$. Although the spectra in figure 1 differ, a heretofore unobserved structure is clearly in evidence at about 130 $cm^{-1}$ (indicated by arrows).

The reflectivity spectra shown in figure 1 were analysed using a fitting procedure based on the modified plasmon–phonon interaction model [9]:

$$\epsilon(\omega) = \epsilon_\infty \left[1 - \omega_p^2/\omega\left(\omega + i\tau^{-1}\right) + \left(\omega_{LO}^2 - \omega_{TO}^2\right)/\left(\omega_{TO}^2 - \omega^2 - i\gamma_{TO}\omega\right) + \omega_{loc}^2/\left(\omega_0^2 - \omega^2 - iG\omega\right)\right] \tag{1}$$

where $\omega_{TO}$, $\omega_{LO}$ and $\omega_p$ are the transverse, longitudinal and plasma frequencies, respectively, $\gamma_{TO}$ is the oscillator damping, $\tau$ is the free-carrier relaxation time and $\epsilon_\infty$ is the high-frequency dielectric constant. The second term in equation (1) is the free-carrier contribution and the third term is the lattice vibration contribution to the dielectric constant. The fourth term in equation (1) represents a new structure in the FIR reflection spectra due to an additional oscillator of characteristic frequency $\omega_0$, where $G$ is the damping and $\omega_{loc}^2$ the 'strength' of this oscillator. The explanation of these parameters will be given below.

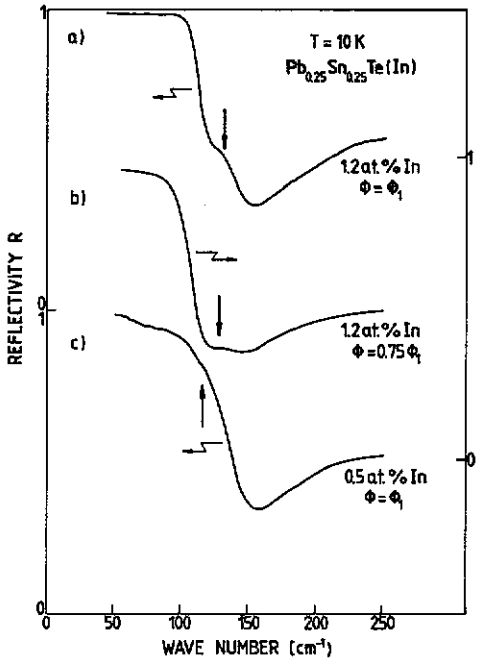


**Figure 1.** FIR reflection spectra of $Pb_{0.75}Sn_{0.25}Te$ (In) single crystals at $T = 10$ K: (*a*) $N_{In} = 1.2$ at.%, $\Phi_1 = \Phi$; (*b*) $N_{In} = 1.2$ at.%, $\Phi_2 = 0.75\Phi$; (*c*) $N_{In} = 0.5$ at.%, $\Phi_3 = \Phi$.

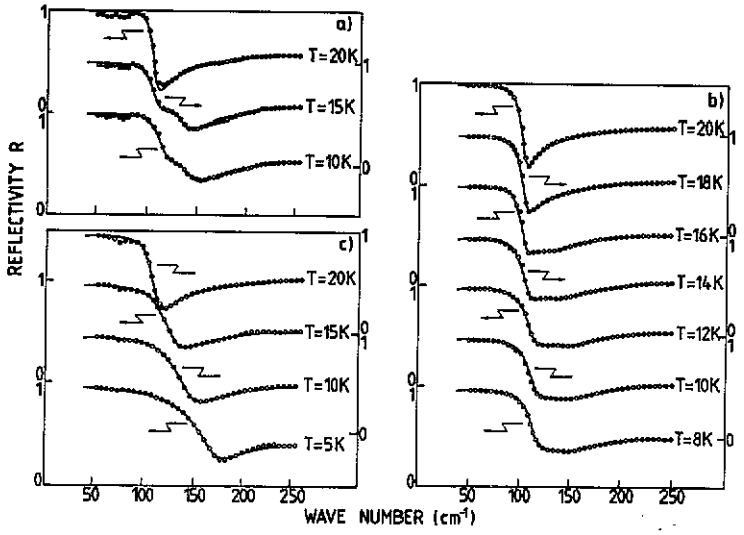


**Figure 2.** FIR reflection spectra of $Pb_{0.75}Sn_{0.25}Te$(In) single crystals at temperatures below $T = 20$ K, showing experimental spectra (○) and calculated spectra (——) obtained by a fitting procedure based on the model given by equation (1), with the parameter values given in table 1: (*a*) $N_{In} = 1.2$ at.%, $\Phi_1 = \Phi$; (*b*) $N_{In} = 1.2$ at.%, $\Phi_2 = 0.75\Phi$; (*c*) $N_{In} = 0.5$ at.%, $\Phi_3 = \Phi$.

As evidenced in figure 2, the computed spectra and experimental data are in reasonably good agreement. The best-fit parameters are listed in table 1. The parameters of the oscillators, $\omega_{TO} = 32$ cm$^{-1}$, $\omega_{LO} = 105$ cm$^{-1}$ and $\gamma = 1$ cm$^{-1}$,

are looked upon as constant because, as we previously discussed [9], their changes in such a narrow temperature interval are negligible. With regard to the fact that the changes $\epsilon_\infty = 44 \pm 2$ and $\tau^{-1} = 38 \pm 4$ cm$^{-1}$ from specimen to specimen in this temperature interval are not great, we have not proceeded to discuss this separately. As can be seen from table 1, the parameter $G$ depending on the In concentration drastically changes from 50 to 100. Moreover, when the flux changes, $\omega_p$ [8, 11] changes, and temperature changes affect $\omega_p$, $\omega_0$ and $\omega_{loc}$.

Table 1 may be used to explain the difference between the spectra in figure 1. As the photo-excited electron concentration $n$ in In-doped $Pb_{0.75}Sn_{0.25}Te$ is defined by the incident light flux, the $n$-value is higher in the case shown in figure 1($a$) than in that in figure 1($b$). This becomes evident if the $\omega_p$-values listed in table 1 for the three cases are compared. Thus, because $\omega_p^2$ is proportional to the total number of free carriers (both impurity and photo-excited), $\omega_{p3}(N_{In} = 0.5$ at.%, $\Phi) > \omega_{p1}(N_{In} = 1.2$ at.%, $\Phi) > \omega_{p2}(N_{In} = 1.2$ at.%, $0.75\Phi)$. This is substantiated in figure 3 which depicts the $\omega_p$–temperature dependence for the three cases discussed.

**Table 1.** Optical parameters of phonons and plasmons obtained by oscillator fitting of the $Pb_{0.75}Sn_{0.25}Te$(In) reflection spectra.

| $T$ (K) | $\omega_p$ (cm$^{-1}$) | $\omega_0$ (cm$^{-1}$) | $\omega_{loc}^2$ (cm$^{-2}$) | $G$ (cm$^{-1}$) | $N_{In}$ (at.%) | $\Phi/\Phi_1$ |
|---|---|---|---|---|---|---|
| 10 | 84 | 135 | 1375 | | | |
| 15 | 71 | 125 | 1275 | 50 | 1.2 | 1 |
| 20 | 36 | 115 | 417 | | | |
| 8 | 73 | 139 | 1128 | | | |
| 10 | 68 | 136 | 1115 | | | |
| 12 | 63 | 133.1 | 1108 | | | |
| 14 | 48 | 127.1 | 1085 | 50 | 1.2 | 0.75 |
| 16 | 35 | 123.2 | 1001 | | | |
| 18 | 25 | 119.5 | 632 | | | |
| 20 | 19 | 115 | 254 | | | |
| 5 | 132 | 146 | 1154 | | | |
| 10 | 103 | 136 | 1132 | | | |
| 15 | 77 | 125 | 1041 | 100 | 0.5 | 1 |
| 20 | 37 | 115 | 347 | | | |

As $\omega_p$ and $\omega_0$ in all three cases lie close to one another, small changes in $\omega_p$ have a great impact on the reflection spectra, i.e. the observability of the additional oscillator in figure 1. That is, for the case depicted in figure 1($a$), $\omega_p$ is lower than $\omega_0$ and a saddle-like structure appears at the plasma edge. As $\omega_p$ increases (figure 1($c$)), the plasma edge masks the additional oscillator, the saddle point becoming almost imperceptible (arrow), and the plasma edge slope changes. If $\omega_p$ is much lower than $\omega_0$ (figure 1($b$)), the additional oscillator is observable but it is not more pronounced because in 'strength' it is the weakest of all those considered (table 1). The values obtained for $\omega_p$ from table 1 are in accordance with the values obtained from transport measurements given in [8, 9, 11].

The $\omega_0(T)$-dependence depicted in figure 4 determines the energy difference between the one-electron and the two-electron states [9]. In figure 4, crosses correspond to the fitted spectra in figure 2($a$), open circles to figure 2($b$) and open

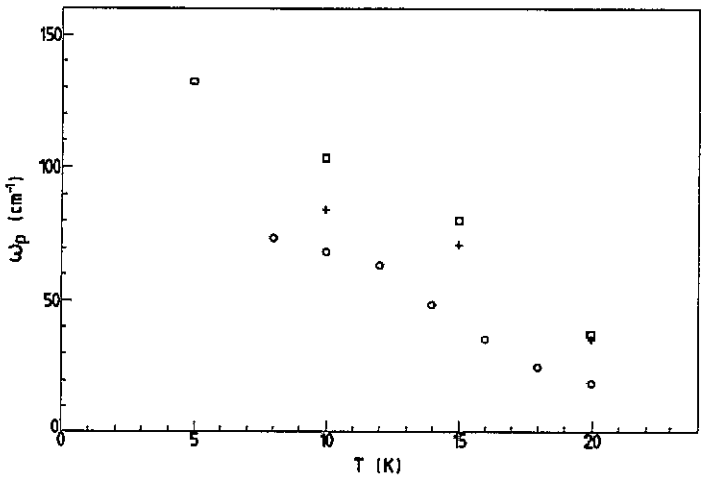


**Figure 3.** Temperature dependence of plasma frequencies: +, $N_{In} = 1.2$ at.%, $\Phi_1 = \Phi$; O, $N_{In} = 1.2$ at.%, $\Phi_2 = 0.75\Phi$; □, $N_{In} = 0.5$ at.%, $\Phi_3 = \Phi$.

squares to figure 2(*c*). An $\omega_0(T) = aT + b$ least-squares linear interpolation yields $a = -2.3 \times 10^{-4}$ eV K$^{-1}$ and $b = 18.2$ meV, $a = \partial\omega_0/\partial T$ being the linear temperature shift coefficient of the energy difference between one- and two-electron states and $b = \omega_0(0)$ the extrapolated energy of the one-electron state at $T = 0$ K.

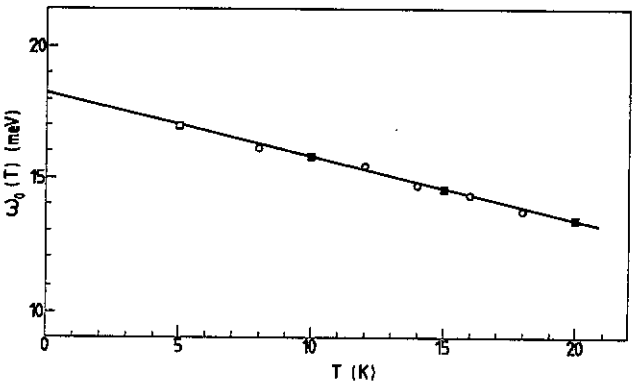


**Figure 4.** Temperature dependence of the additionally introduced oscillator characteristic frequency $\omega_0$: +, $N_{In} = 1.2$ at.%, $\Phi_1 = \Phi$; O, $N_{In} = 1.2$ at.%, $\Phi_2 = 0.75\Phi$; □, $N_{In} = 0.5$ at.%, $\Phi_3 = \Phi$.

The $\omega_{loc}^2(T)/\omega_{loc}^2(0)$ curve is given in figure 5, with the same notation as in figure 3 for the experimental data. The oscillator strength $\omega_{loc}^2$ is a function of the electron transition rate between the two-electron and one-electron localized states. It is easy to show that the normalized value $\omega_{loc}^2(T)/\omega_{loc}^2(0)$ is proportional to the temperature-dependent part on the transition matrix element $M_{12}^2$. The value of $M_{12}^2$ is in turn determined by the one-electron (excited) state lifetime $\tau_1$ [12]. $\tau_1$ depends on the probability $W_e$ of electron emission from the one-electron state as $\tau_1 \sim 1 - W_e$. At low temperatures this emission is defined in terms of thermal activation via the barrier ($E_g$) between the one-electron ($E_1$) and two-electron ($E_2$)

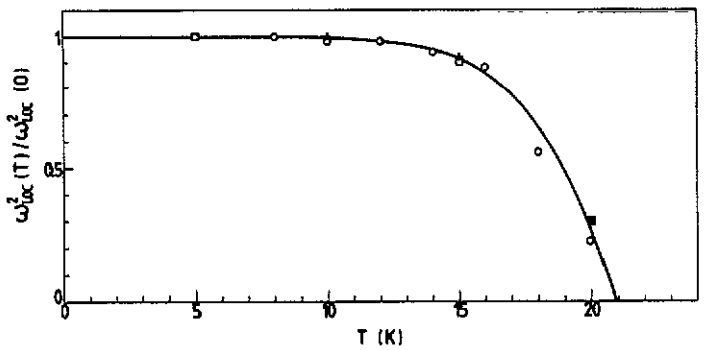


**Figure 5.** Temperature dependence of normalized 'strength' $\omega^2_{loc}(T)/\omega^2_{loc}(0)$ of the additionally introduced oscillator: +, $N_{In} = 1.2$ at.%, $\Phi_1 = \Phi$; ○, $N_{In} = 1.2$ at.%, $\Phi_2 = 0.75\Phi$; □, $N_{In} = 0.5$ at.%, $\Phi_3 = \Phi$.

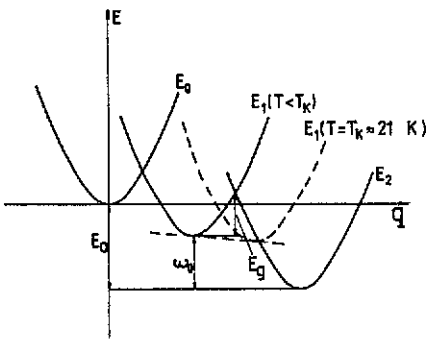


**Figure 6.** Configuration coordinate diagram for indium in $Pb_{0.75}Sn_{0.25}Te$.

localized states $W_e = \exp(-E_g/kT)$ (figure 6).

According to our scheme, the curve corresponding to the one-electron state moves as the temperature rises, and at $T = T_k$, the barrier between states $E_1$ and $E_2$ disappears (see the broken curve in figure 6). A good fit (full curve in figure 5) is obtained for

$$\omega^2_{loc}(T)/\omega^2_{loc}(0) = 1 - \exp(-E_g/kT) \tag{2}$$

where $E_g$ is the two-electron-to-one-electron-state barrier width (see figure 6). A linear $E_g$–temperature dependence $E_g = A(T_k - T)$ results in a best-fit parameter of $E_g(\text{meV}) = 0.56(21 - T)$. Note that the value of $T_k = 21$ K coincides with the persistent photoconductivity temperature obtained from galvanomagnetic measurements [2, 8, 9, 11]. One can see that, at liquid-helium temperature, $E_g \gg kT$. Nevertheless, measurements of long-term photoconductivity relaxation show that the redistribution of the localized-state occupancies during this process plays an important role [13]. This means that at temperatures $T < 10$ K the main contribution to the transitions between $E_1$ and $E_2$ comes from tunnelling through the barrier $E_g$.

The universality of the $\omega^2_{loc}(T)/\omega^2_{loc}(0)$ curve indicates that the temperature-dependent part of the transition matrix element does not depend on the experimental conditions (light flux), nor does the interaction of the impurity centres affect the temperature-dependent part of intercentre transitions.

The impurity centre configuration state diagram is shown in figure 6. In accordance with the $\omega_0(T)$-dependence, the energy of the minimum that corresponds to the one-electron state is near the bottom of the conduction band (state $E_1$ in figure 6). The $E_1$-state occupancy is strongly temperature dependent ($\omega^2_{loc}(T)$), indicating a change in the barrier width between $E_1$ and $E_2$. At $T_k = 21$ K this barrier vanishes (broken curve in figure 6) and the related $\omega^2_{loc}$ drops to zero. The coincidence of this temperature with the temperature of the onset of the persistent photoconductivity effect supports our assumption that persistent photoconductivity depends on non-equilibrium charge-carrier relaxation via the one-electron metastable localized state.

## 4. Conclusion

The measurements of FIR reflectivity spectra discussed were performed on In-doped $Pb_{0.75}Sn_{0.25}Te$ single crystals in the temperature range 5–20 K for a variety of doping concentrations. We have shown that persistent conductivity depends on photo-excited electron relaxation via the metastable one-electron state. At $T < 21$ K, this state lies below the bottom of the conduction band and above the stable two-electron state. The potential barrier ($E_g(0) = E_{g0} = 11.76$ meV at $T = 0$ K) between these two states and its temperature dependence have been determined. The existence of the barrier is a pre-condition for the appearance of the persistent photoconductivity effect. We have also determined the position of the metastable one-electron in respect to the two-electron state ($\omega_0$ at $T = 0$ K) and its temperature dependence.

## Acknowledgments

The authors thank W König for the measurement of the FIR spectra, and A V Nikorich for samples.

## References

[1] Ravich Yu I, Efimova B A and Smirnov I A 1970 *Semiconducting Lead Chalcogenides* ed L S Stil'bans (New York: Plenum) p 60
[2] Akimov B A, Ryabova L I, Yatsenko O B and Chudinov S M 1979 *Fiz. Tekh. Poluprov.* **13** 752 (Engl. Transl. 1979 *Sov. Phys.–Semicond.* **13** 441)
[3] Lent C S, Bowen M A, Allgaier R S, Dow J D, Sankey O F and Ho E S 1987 *Solid State Commun.* **61** 83
[4] Vul M, Voronova I D, Kalyuzhnaya G M, Mamedov T S and Ragimova T Sh 1979 *Zh. Eksp. Teor. Fiz. Pis. Red.* **29** 21 (Engl. Transl. 1979 *JETP Lett.* **29** 18)
[5] Adler P and Yoffa E J 1976 *Phys. Rev. Lett.* **36** 1197
[6] Akimov B A, Brandt N B, Klimonskiy S O, Ryabova L I and Khokhlov D R 1982 *Phys. Lett.* A **88** 483
[7] McKnight S W and El-Rayess M K 1984 *Solid State Commun.* **49** 1001
[8] Romčević N, Popović Z V, Khokhlov D R, Nikorich A V and König W 1991 *Infrared Phys.* **31** 225
[9] Romčević N, Popović Z V, Khokhlov D R, Nikorich A V and König W 1991 *Phys. Rev.* B **43** 6712
[10] Akimov B A, Brandt N B, Nikorich A V, Ryabova L I and Sokovishin V V 1984 *Zh. Eksp. Teor. Fiz. Pis. Red.* **39** 222 (Engl. Transl. 1984 *JETP Lett.* **29** 198)
[11] Akimov B A, Albul A V, Nikorich A V, Ryabova L I and Khokhlov D R 1984 *Fiz. Tekh. Poluprov.* **18** 1778 (Engl. Transl. 1984 *Sov. Phys.–Semicond.* **18** 1112)

[12] Ravich Yu I, Efimora B A and Smirnov I A 1970 *Semiconducting Lead Chalcogenides* ed L S Stil'bans (New York: Plenum) p 88

[13] Ivanchik I I, Khokhlov D R, Nikorich A V, Popović Z V and Romčević N 1990 *Proc. 8th Int. Conf. on Ternary and Multinary Compounds (Kishinev, 1990)* p 318